The Predictability of the Extratropical Flow Response to Recurving Atlantic Tropical Cyclones

ALLISON LYNN BRANNAN[a] AND JEFFREY M. CHAGNON[a]

[a] *Florida State University, Tallahassee, Florida*

(Manuscript received 1 October 2020, in final form 7 May 2021)

ABSTRACT: Given the ability of recurving Atlantic tropical cyclones (TCs) to disturb the amplitude of Rossby waves on the extratropical jet, this study investigates whether the predictability of the synoptic-scale flow is significantly modified from climatology downstream from and after TC recurvature events. Predictability is evaluated as the standard deviation of isentropic potential vorticity among a 50-member ensemble and is compared with a model climatology. It is shown that forecast uncertainty is dependent upon the relative location of the nearest trough at the time of recurvature and the relative zonal speed between the aforementioned trough and the TC in the 72 h after recurvature. Predictability is significantly degraded when recurvature occurs downstream of a trough; the elevated uncertainty subsequently propagates downstream along with the trough axis. Furthermore, this study evaluates predictability in spectral space to distinguish between uncertainty tied to the exact location of troughs and ridges and uncertainty in Rossby wave amplitude. The wavelet analysis demonstrates that the increase in uncertainty is not solely limited to the trough location, as there is also significantly elevated uncertainty in the Rossby wave amplitude that originates from the upstream trough and spans across downstream troughs and ridges. Uncertainty is also increased near the recurvature longitude in the subset of cases in which the Rossby wave train propagates zonally slower than the TC after recurvature, which is hypothesized to be linked to baroclinic growth processes.

KEYWORDS: Rossby waves; Wavelets; Tropical cyclones; Ensembles

1. Introduction and background

Tropical cyclones (TCs) in the Atlantic basin regularly attain latitudes poleward of 35°N, which situates them on the west/northwest side of the subtropical high and in a position susceptible to the steering flow of the midlatitude jet. These large-scale circulation features often cause the TCs to begin moving northeastward as opposed to their original northwestward-directed track, which is commonly referred to as ''recurvature.'' Approximately 1–2 days following recurvature (Aiyyer 2015; Torn and Hakim 2015), a process known as ''extratropical transition'' begins as the midlatitude temperature gradients provoke the TCs to lose their tropical characteristics and acquire structures of extratropical cyclones (Jones et al. 2003). While the extratropical flow is able to influence the TC's track and structure, these TCs are also capable of disturbing and modifying the Rossby waves on the midlatitude jet, which has implications for severe and extreme weather events downstream (Harr and Dea 2009; Cordeira and Bosart 2010; Grams et al. 2011; Archambault et al. 2013; Grams et al. 2013a; Pantillon et al. 2013; Archambault et al. 2015; Grams and Archambault 2016; Pohorsky et al. 2019). Although the extratropical flow response is not consistent following every Atlantic TC recurvature, the variation in the downstream extratropical flow response is most strongly connected to the average Rossby wave relative speed of the recurving TC within the 72 h following recurvature (Brannan and Chagnon 2020). The cases in which the trough closest to the TC's recurvature point moves zonally faster than the TC after recurvature are those most likely to yield amplified synoptic-scale Rossby waves downstream from recurvature. Conversely, recurvature events in which the TC outruns its nearest trough have been associated with a brief period of synoptic-scale Rossby wave suppression. The significant change in Rossby wave amplitude downstream from the recurving TC motivates this study to determine if this TC–jet interaction introduces or elevates the uncertainty of downstream weather forecasts and if the predictability of the downstream weather is sensitive to the characteristics of the recurving TC or its phasing with the jet.

Deterministic numerical weather prediction is an initial value problem requiring accurate and precise specification of the current state of the atmosphere as well as a flawless model in order to generate a reliable prediction of a future state. With increasing lead time, small errors in the estimation of the initial state grow, thus rendering forecasts less accurate. Lorenz (1965) revealed that forecasts proceeding from initial conditions that varied only infinitesimally from each other would eventually diverge until all initial condition information is lost and the average difference between the solution states is as large as the average difference between randomly selected solution states, representing the ''limit'' to deterministic predictability. Lorenz (1995) hypothesized that this limit on predictability is a function of the dynamical system, the available observations, and the model's ability to simulate the system.

Predictability may be quantified in numerical weather prediction studies through the use of ensembles in which small perturbations to the initial conditions and stochastic perturbations of the parameterizations produce an assortment of possible outcomes. The predictability of this ensemble of simulations can be evaluated on the basis of 1) bias, measured by the errors from observations or reanalyses and 2) the uncertainty, typically quantified by the variance among the ensemble members. Forecasts with substantial errors are poor representations of the future state, corresponding to either events with low predictability or a low predictive skill.

Corresponding author: Allison Lynn Brannan, albrannan@gmail.com

DOI: 10.1175/MWR-D-20-0325.1

Separately, a large spread, or a large variance, between ensemble members indicates a regime with greater forecast uncertainty and is therefore linked to reduced predictability (Harr et al. 2008; Anwender et al. 2008, 2010).

Our current numerical weather prediction models experience difficulties simulating the structural changes of extratropical transitioning TCs even at short lead times (Evans et al. 2006). Furthermore, the representation of midlatitude Rossby waves (including their amplitude, location, and phasing with the TC) contributes additional variability, yielding a degree of medium- to extended-range forecast uncertainty surrounding TC recurvature and the resulting large-scale flow. These errors tend to grow and propagate, leading to additional and/or increased forecast errors in the evolution of the downstream waveguide and downstream extreme weather (Jones et al. 2003; Harr et al. 2008; Anwender et al. 2008; Reynolds et al. 2009; Anwender et al. 2010; Pantillon et al. 2013; Quinting and Jones 2016). Therefore, small errors in the forecast of the TC (e.g., track, intensity, etc.) or the forecast of the large-scale flow (e.g., strength of the potential vorticity (PV) gradient, position of the jet, location or amplitude of troughs/ridges, etc.) may cause greater uncertainty in downstream weather, as exemplified by case studies of individual recurvature events (Jones et al. 2003; Anwender et al. 2008; Harr et al. 2008; Reynolds et al. 2009; Anwender et al. 2010; Chaboureau et al. 2012; Pantillon et al. 2013).

Several studies have examined climatologies of forecasts following recurving TCs within the western North Pacific, Atlantic, and southern Indian Ocean basins. Using the ensemble standard deviation of either 250- or 500-hPa geopotential heights to quantify predictability, Aiyyer (2015), Quinting and Jones (2016), and Torn (2017) agree that the most prominent departure from climatology occurs in the North Pacific basin where a statistically significant widening of the ensemble spread emerges near the time of recurvature and along the recurvature longitude. This decreased predictability propagates with the group velocity of the Rossby waves into the downstream regions, following TC recurvature (Harr et al. 2008; Anwender et al. 2008; Pantillon et al. 2013; Aiyyer 2015; Quinting and Jones 2016; Torn 2017). The role of forecast lead time was also evaluated within these studies. Based on the results from Aiyyer (2015) and Torn (2017), it appears that recurvature events abruptly increase the ensemble spread downstream from recurvature regardless of the forecast lead time. However, the largest positive standard deviation anomalies downstream of the recurvature event are found in forecasts initialized in the days leading up to recurvature, but actually decrease back toward climatology in the days following recurvature (Torn 2017). This result highlights the idea that the uncertainties surrounding the recurvature event are communicated into the downstream forecasts until the recurvature details (e.g., phasing with upstream trough, timing of recurvature, etc.) are accurately represented within the initial conditions (Torn 2017).

Nevertheless, the unique factors of the TC–jet interaction that act as the sources of uncertainty throughout the recurvature time period and the resulting downstream flow still remain unclear. The numerical weather prediction forecast uncertainty following a TC recurvature/jet interaction has been predominantly hypothesized to originate from either 1) errors stemming from inaccuracies in representing the phasing between the recurving TC and its upstream trough (Klein et al. 2002; Anwender et al. 2008; Harr et al. 2008; Riemer and Jones 2010; Grams et al. 2013b) or 2) the inability to explicitly capture the effects of the TC's upper-level divergent outflow on the jet stream's inherent PV gradient (Riemer et al. 2008; Harr and Dea 2009; Keller et al. 2014; Archambault et al. 2015). The results from Torn (2017) show that the cases with the greatest downstream uncertainty are those with highly amplified ridges downstream from the TC recurvature point. These results, though, are in opposition to those from Aiyyer (2015) who reported a slight increase in predictability (decrease in ensemble spread) for cases where North Pacific TC recurvatures yield an enhanced downstream ridge. Other characteristics such as the presence of an upstream trough, the forecast variance of TC position, the magnitude of latent heat release, and the amount of PV advection by the TC's upper-level divergent outflow have been cited as insignificant factors in determining the degree of downstream forecast uncertainty (Torn 2017).

The purpose of this study is to elaborate on the previous climatologies that have examined the effects of recurving Atlantic TCs on the downstream, large-scale predictability. Previous studies (Aiyyer 2015; Quinting and Jones 2016; Torn 2017) have examined the standard deviation of 250- or 500-hPa geopotential heights to assess trends in predictability throughout recurvature periods. This study, however, will evaluate predictability through an analysis of PV on the 320-K isentropic surface throughout the Atlantic basin during TC recurvature periods. The complete set of Atlantic recurvature cases will be subdivided based on characteristics of the TC, the large-scale flow, and the interaction between the two in order to determine which characteristics, if any, produce statistically significant differences in downstream predictability. The novel aspects of this analysis distinguishing it from previous studies are as follows. 1) The focus on isentropic PV (as opposed to geopotential heights) highlights the influence of TC recurvature on the large-scale Rossby wave response. 2) A wavelet technique is used in order to distinguish between the uncertainty in the amplitude of the wave pattern and the uncertainty in the location of troughs and ridges. 3) Following the conclusion of Brannan and Chagnon (2020), this study considers the role of the relative propagation speed of the recurving TC versus the nearest trough in regulating the predictability, rather than focusing exclusively on the relative location of each feature at the time recurvature.

The remaining sections of this paper are presented as follows. Section 2 describes the data sources, the metric for characterizing Rossby waves, and the method of quantifying predictability. Section 3 begins with a full composite analysis of the PV standard deviation anomalies, which are then subdivided based on various recurvature characteristics to determine which of these yield the largest differences in downstream predictability. A similar analysis of predictability is then executed within spectral space in section 4. Conclusions are discussed in section 5 along with insight into future extensions of this study.

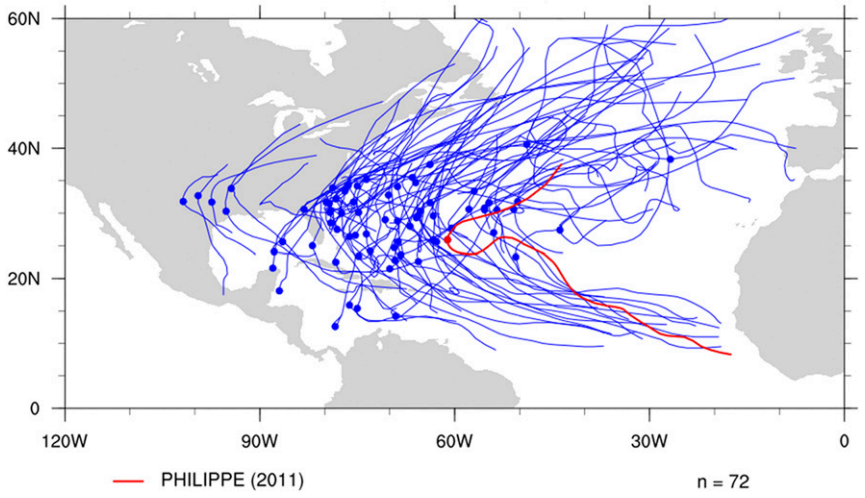

FIG. 1. Tracks of the 72 recurving Atlantic Ocean TCs that occurred between 2007 and 2016 and reached a latitude of 35°N. Dots indicate the recurvature point of each track. The red track represents TC Philippe (2011), which is used in Fig. 2 to demonstrate the Rossby wave detection methods.

2. Data and method

To analyze the predictability associated with recurving Atlantic TCs, this study requires a poststorm reanalysis dataset including tracks and descriptive characteristics of historical recurving TCs as well as operational analyses and ensemble forecasts of the PV field throughout the Atlantic basin before, during, and after TC recurvature. Furthermore, the wavelet power decomposition technique and analysis rely on a variant of the ensemble PV field as a metric to characterize the extratropical jet, all of which are described in the following section.

a. Data and sources

Rossby waves on the extratropical jet propagate as undulations in PV on isentropic surfaces. For each Atlantic TC recurvature event included in this study, PV on the 320-K isentropic surface on a $1° \times 1°$ global grid is obtained as both operational analyses and historical forecasts from the European Centre for Medium-Range Weather Forecasts (ECMWF) through the THORPEX Interactive Grand Global Ensemble (TIGGE) Data Retrieval archive (Swinbank et al. 2016), which includes data dating back to 2006. These ECMWF forecasts contain 50 ensemble members. Forecast data are acquired for initialization times ranging from 10 days (240 h) before each TC's recurvature to 10 days (240 h) after recurvature, with forecast output at 12-h intervals and forecast cycles that extend 15 days (360 h) after initialization. Forecasts are initialized at 0000 and 1200 UTC each day.

To the authors' knowledge, this study is the first to evaluate the predictability of downstream Rossby waves following Atlantic TC recurvature events using PV on an isentropic surface for tracking and quantification. PV is conserved following frictionless, adiabatic flow, making it a worthy tracer of the large-scale flow on an isentropic surface (Hoskins et al. 1985). The meridional gradient in PV provides the restoring force responsible for the propagation of Rossby waves, often referred to as the midlatitude waveguide (Martius et al. 2010). Therefore, contrary to previous studies that analyzed geopotential heights, the unique characteristics of PV on an isentropic surface render it better suited for diagnosing the structure and behavior of upper-level Rossby waves on the extratropical jet, downstream from a recurvature event. The 320-K isentropic surface is chosen for this study for consistency with a previous study (Brannan and Chagnon 2020), but also because it regularly intersects the midlatitude tropopause near the latitude location of the extratropical jet stream.

Recurving TC tracks along with descriptive characteristics throughout the TC's life cycle are extracted from HURDAT2, which is a best track reanalysis database from the National Hurricane Center containing information on all Atlantic TCs dating back to 1851 (Landsea and Franklin 2013). This dataset is a poststorm reanalysis that provides data on each TC's position, central pressure, size based on the 34-kt ($1\ \text{kt} \approx 0.51\ \text{m s}^{-1}$) wind speed radii, and maximum sustained winds at regular 6-h intervals.

Storms are selected as recurving TCs if they possess three consecutive time steps where the storm tracks eastward and northward. This procedure, therefore, also allows the inclusion of TCs that lack an initial westward track component, but begin their life cycle moving in the northeast direction as commonly seen from TCs developing in the Caribbean or Gulf of Mexico. Additionally, this study requires that each TC reaches a latitude of 35°N, to ensure that it attains a position with a reasonable chance of interaction with the midlatitude jet stream. Last, recurving TC cases are limited to those storms that occurred between 2007 and 2016 in order to align with the available archived forecast data. These criteria result in a total of 72 recurving Atlantic TCs to be analyzed in this study, whose tracks are displayed in Fig. 1.

The method of identifying the recurvature point is identical to that performed in Brannan and Chagnon (2020). The recurvature point is selected as the westernmost point attained

by the TC before its redirection toward the east. One caveat to note is that recurvatures occurring at 0600 or 1800 UTC are adjusted to the previous point at 0000 or 1200 UTC, respectively, in order to account for the differences in time intervals between HURDAT2 and TIGGE (6-h intervals in HURDAT2 while only 12-h intervals in TIGGE).

To determine the effects of a recurving TC on the predictability of the downstream synoptic-scale flow, TC tracks are aligned based on their recurvature time and longitude to fairly separate before and after recurvature, as well as upstream from downstream, when compositing across the group of TCs (Aiyyer 2015; Quinting and Jones 2016). In this recurvature-relative framework, a longitude of 0 corresponds to the recurvature longitude and a time of 0 coincides with the recurvature time for each individual case. Therefore, negative longitude values are located upstream from the TC's recurvature point and positive longitude values are downstream of the TC's recurvature point. Similarly, time values less than zero denote hours before recurvature occurs and positive time values represent hours after recurvature. There is not a clear definition for the exact time when interaction between the TC and the extratropical jet begins. Several studies (e.g., Archambault et al. 2015; Aiyyer 2015; Quinting and Jones 2016) have used the recurvature time for normalization between TCs, some (e.g., Torn 2017) have suggested the use of the onset time of extratropical transition, while others (e.g., Archambault et al. 2015) have used the point of maximum interaction defined by the point of strongest negative PV advection by the TC's irrotational wind. Given the ambiguity concerning the onset time for interaction, a reasonable estimate for the uncertainty associated with this choice is approximately 36 h. Because we seek to identify signals that persist for longer than two days, this uncertainty is acceptable.

b. Rossby wave diagnosis

The location and amplitude of Rossby waves on the extratropical jet must be diagnosed 1) to "subset" the full group of TCs by phasing characteristics between the TC and the midlatitude Rossby waves (section 3c) and 2) to perform a wavelet spectral decomposition that allows an isolated analysis of the predictability of Rossby wave amplitude (section 4). Rossby waves are identified here by the same technique used in Brannan and Chagnon (2020). This technique is summarized here and elaborated in Brannan and Chagnon (2020). Between 40° and 70°N, a meridional average of PV is calculated, yielding a single value of mean PV at each longitude that is subsequently converted to an anomaly from the global midlatitude mean PV. To filter any subsynoptic-scale disturbances, a spatial filter is applied using a weighted running average of these anomalies. The resulting "Rossby wave metric" is capable of reliably diagnosing the location and relative amplitude of troughs and ridges on the extratropical jet, which is demonstrated for a single time following the recurvature of TC Philippe (2011) by plotting the Rossby wave metric alongside the PV field in Fig. 2a. The 1.5 potential vorticity unit (1 PVU = $10^{-6}\,\mathrm{K\,kg^{-1}\,m^2\,s^{-1}}$) contour is used here to estimate the latitude of the extratropical jet stream on the 320-K isentropic surface (Nielsen-Gammon 2001). To facilitate a visual comparison with the 1.5-PVU contour, the Rossby wave metric is translated, inverted, and magnified according to the figure caption, though the raw Rossby wave metric is used for all calculations. Despite some limitations, the Rossby wave metric reliably captures the trough and ridge locations along with their relative amplitudes, allowing it to be used for a wavelet spectral decomposition described in the following section.

c. Wavelet decomposition

Brannan and Chagnon (2020) used wavelet spectral analysis (Torrence and Compo 1998) to diagnose the location, amplitude, and wavelengths of Rossby waves during TC recurvature events. The same technique is used in this analysis of predictability. Wavelet transforms are applied to the PV-based Rossby wave metric described in section 2b. A strength of the technique is that it distinguishes amplitude from phase in physical space, meaning that slight zonal translations of individual troughs and ridges imbedded within the large-scale wave pattern will not affect the wavelet power at a specific location and wavelength. In other words, we may separately evaluate the forecast uncertainty attributed to the amplitude of the wave pattern versus that associated with the location of trough/ridge axes (section 4).

The reliability of this wavelet decomposition technique in detecting the power and location of troughs is shown for the time 48 h after the recurvature of TC Philippe (2011) in Fig. 2b. The lack of power in the shortest wavelengths can be attributed to the spatial averaging implemented during the calculation of the Rossby wave metric, which smoothed and filtered subsynoptic-scale perturbations. Each trough present in the raw PV field of Fig. 2a corresponds to a region of synoptic-scale trough power as identified by the wavelet decomposition technique in Fig. 2b. Ridges (not shown) are also clearly captured by the wavelet decomposition method. The analysis of predictability in spectral space (section 4) focuses on synoptic-scale wavelengths, defined in this study as an average over 20°–60° wavelengths, which are plotted in Fig. 2c.

d. Assessment of predictability

This study will evaluate the uncertainty of medium-range, synoptic-scale forecasts through both physical and spectral lenses while using similar forecast evaluation techniques. The first half of this study (section 3) resides in physical space and analyzes forecasts of raw PV in the Atlantic basin. Section 4 focuses on spectral space by evaluating the wavelet power in 20°–60° wavelengths of the forecast Rossby wave metric. It should be noted that the remainder of this section solely refers to the "wavelet power" in the description of the methods; however, these procedures are applied to the total wavelet power spectra, as well as the trough power spectra and the ridge power spectra separately.

Predictability will be characterized by the standard deviation of the distribution of PV (section 3) or synoptic-scale wavelet power (section 4) between the 50 ensemble members, which is calculated for each lead time over every forecast cycle. The goal is to identify locations and times where and when the forecast uncertainty is significantly modified during a TC recurvature event. With or without TC recurvature, the ensemble's standard deviation is expected to increase as a function of

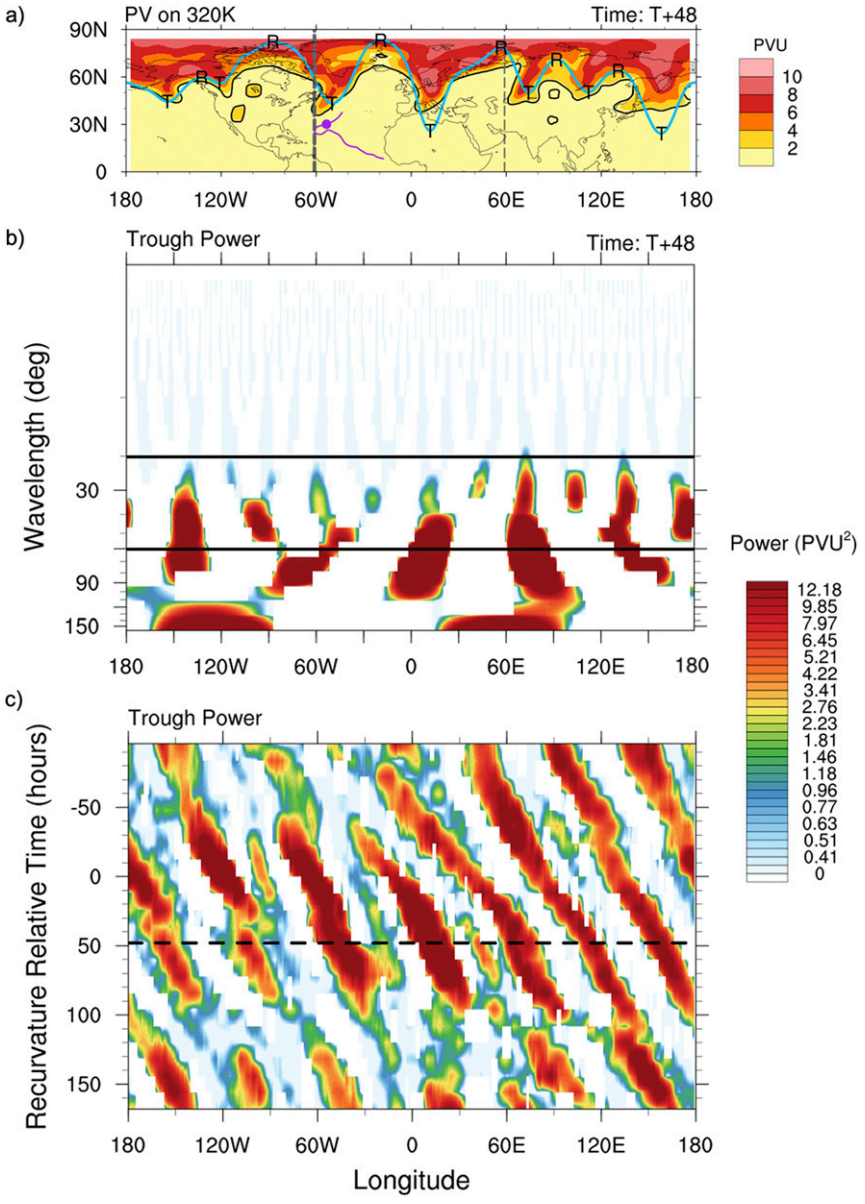

FIG. 2. A demonstration of the Rossby wave metric and the wavelet power spectrum at 0000 UTC 8 Oct 2011, corresponding to 48 h after the recurvature of TC Philippe. (a) Potential vorticity on the 320-K isentropic surface (color shading); the 1.5-PVU contour (black), which can be used to approximate the location of the jet stream; and the Rossby wave metric (blue), which has been inverted, translated north by 60°, and amplified by a factor of 10 to facilitate comparison with the 1.5-PVU contour. The purple line shows the complete track of TC Philippe, with the purple dot indicating the position at this individual time. The thick gray dashed line denotes the longitude of recurvature, and the thin gray dashed line denotes 120° downstream of the recurvature longitude. Here, T indicates a trough location and R indicates a ridge. (b) Trough power as calculated by the wavelet decomposition technique. This study focuses on 20°–60° wavelengths, which are those wavelengths between the horizontal black lines. (c) Trough power averaged over synoptic-scale wavelengths (20°–60°) and plotted over times from 96 h before recurvature to 168 h after recurvature. The black dashed line denotes 48 h after recurvature, corresponding to the time of (a) and (b).

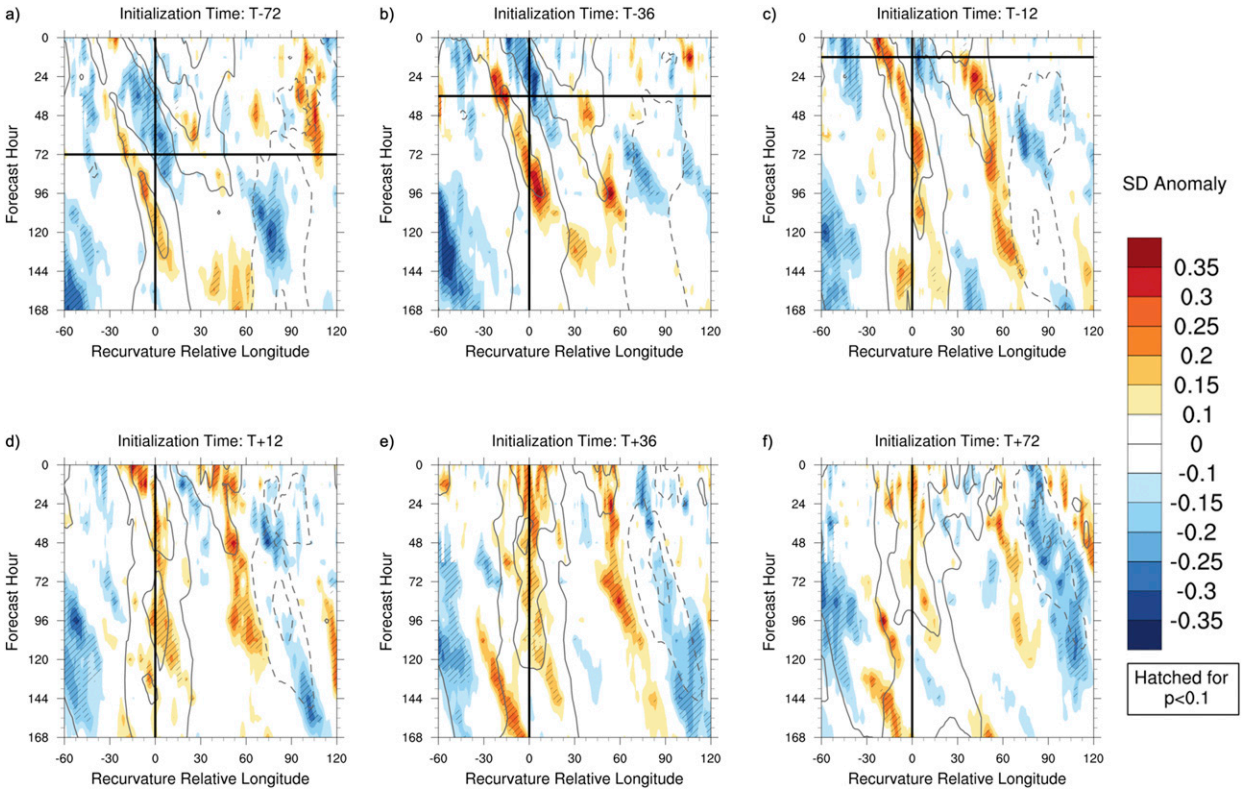

FIG. 3. Color shading displays the normalized standard deviation anomalies of PV on the 320-K isentropic surface, averaged between 40° and 70°, for all 72 Atlantic recurvature events and forecast cycles initialized at (a) 72 h before, (b) 36 h before, (c) 12 h before, (d) 12 h after, (e) 36 h after, and (f) 72 h after recurvature. The thick vertical and horizontal lines denote the recurvature longitude and time, respectively. Hatching indicates times/locations where anomalies are statistically significant from climatology at the 90% confidence level. Average PV is also plotted, with 1.6 and 1.8 PVU shown by dashed gray contours and 2.2 and 2.4 PVU shown by solid gray contours.

lead time and to vary by location. To detect a signal associated with TC events, the standard deviations across the ensemble are normalized by a "climatology" that is a function of the time of year, forecast lead time, and physical (as opposed to recurvature-relative) longitude. This reference climatology is calculated from the simulated PV (or wavelet power) encompassed by all 42 initialization times/forecast cycles that straddle (±10 days) each recurvature date of the 72 TCs examined in this study. This PV climatology operates on a meridional average from 40° to 70°N and maintains the full range of geographic longitudes (from −180° to 179°E). The wavelet climatology acts on a synoptic-scale wavelength average (20°–60°) but also spans the same range of geographic longitudes. Both climatologies are calculated according to the month of each forecast verification time, which is subsequently interpolated linearly to a daily value. The ensemble standard deviation of PV (or wavelet power) for each case is normalized by the daily climatology using the following calculation, which is analogous to a z-score:

$$\text{normalized\_}\sigma = \frac{\sigma(i,f,l) - \overline{\sigma_{\text{climo}}(v,f,l)}}{\sigma_{\sigma_{\text{climo}}}(v,f,l)}, \qquad (1)$$

where σ is the ensemble standard deviation of PV (or wavelet power) for an individual forecast cycle at initialization time i, lead time f, and natural longitude l. Here, $\overline{\sigma_{\text{climo}}}$ denotes the average climatological forecast standard deviation of PV (or wavelet power) at the verification time v (where $v = i + f$), lead time f, and natural longitude l, and $\sigma_{\sigma_{\text{climo}}}$ is the standard deviation of the climatological forecast standard deviation of PV (or wavelet power) at the given verification time v, lead time f, and natural longitude l. After these pseudo z-scores are calculated to normalize the ensemble standard deviations of PV across the Atlantic basin, the natural longitude values l and initialization times i are then shifted to recurvature relative coordinates to illuminate systematic downstream and post-recurvature trends in the ensemble standard deviation across the full set of TCs. The t tests are executed using 2000 random bootstrap replications to determine whether the normalized standard deviation values are significantly different from the climatology at the corresponding time and location at the 95% confidence level.

3. Physical space results

a. Composites over all TCs

Forecasts centered in both time and longitude on the TC's recurvature demonstrate predictability patterns that are anchored in time and space to the TC recurvature event. Figure 3

displays composites from the 72 Atlantic recurving TC cases of normalized forecast ensemble standard deviation anomalies throughout the recurvature time period as a function of forecast lead time and recurvature relative longitude for several different recurvature relative initialization times. As shown in Figs. 3a–e, an area of standard deviation that is significantly greater than climatology (lower-than-average predictability) emerges approximately 12 h before and 30° upstream of the recurvature event and is forecast to propagate downstream with time for several days beyond the recurvature time. Though plots from previous initialization times are not shown here, this above-average standard deviation anomaly and its downstream propagation is consistent in verification time, location, and magnitude back through initialization times of $T - 168$ h (168 h before recurvature). Notice that as the initialization times approach the recurvature time ($T + 0$ h), the position of this positive standard deviation anomaly is anchored to the recurvature verification time. This plume of enhanced standard deviation is tied to the timing of the recurvature event regardless of forecast lead times. The consistency of the positive standard deviation anomaly's magnitude demonstrates that the standard deviation normalization technique described in section 2d facilitates a fair comparison over the range of forecasts hours. These persistent magnitudes also imply that the predictability of the PV distribution in the Atlantic basin and downstream is not improved by merely initializing closer to recurvature time, which is consistent with the findings from Torn and Hakim (2015), Aiyyer (2015), and Torn (2017). This finding highlights the tie between the downstream uncertainty and the recurvature event itself. In the three shown initialization times before recurvature (Figs. 3a–c) as well as those extending back to $T - 168$ (not shown), there is also evidence of below-average ensemble standard deviation. The signal emerges approximately 48 h before and 20° upstream of recurvature and subsequently extends downstream until reaching about 15° east of the recurvature longitude at 12 h after recurvature. This couplet of significantly above- and below-average standard deviation of the ensemble PV forecasts near the recurvature longitude appears to be related to the average longitudinal locations of the nearest trough and ridge, respectively, at the time of recurvature, which is consistent with the results from Torn (2017) and investigated further in section 4. At an initialization time 12 h before recurvature (Fig. 3c), a second area of decreased predictability (increased standard deviation) emerges 30° downstream from the recurvature longitude, beginning at the recurvature verification time and subsequently propagates downstream aligned with a second trough axis. The magnitude of this second positive anomaly is comparable to the previously mentioned positive anomaly originating upstream before recurvature. The anomalies are consistent through initialization times up to $T + 48$ h (Figs. 3c–e), after which their magnitudes decrease (Fig. 3f).

These results align well with those presented for the Atlantic basin by Torn (2017) who used a similar method to normalize the standard deviation of 500-hPa heights as a proxy for predictability. Both studies found areas with alternating signs of above- and below-average ensemble standard deviations beginning near the time and longitude of recurvature, regardless of the initialization time, which propagate downstream aligned with a Rossby wave pattern. While the magnitudes of the signals are comparable between the studies, differences are seen in the breadth of the signals, especially as they propagate downstream. The areas of decreased predictability in this study propagate downstream while maintaining a fairly constant longitudinal width, whereas the areas of decreased predictability in the Torn (2017) analysis expand in longitudinal extent. The lack of expansion on the edges of this area of decreased predictability may imply a nondispersive error-wavepacket, although a formal diagnosis has not been executed by this study.

b. *Composites over subsets based on TC characteristics*

While statistical significance was identified in the composite analysis of the complete set of TCs considered in this study, it is not expected that all TCs interact with the extratropical flow in the same way. This section will present composites of events that were subgrouped according to various characteristics of the TC and the large-scale flow. The subgroups are based on the highest and lowest terciles of the TC's minimum central pressure (Fig. 4a), maximum sustained wind speed (Fig. 4b), size of the average 34-kt wind radii (Fig. 4c), latitude (Fig. 4d), and day of year (Fig. 4e) at the time of recurvature, as calculated from the HURDAT reanalysis. Terciles are used in this study as opposed to quartiles to increase the sample size of the subsets while still focusing on cases that are well above or below the average. Additional subgroups are created on the basis of positive and negative Rossby wave relative location at the time of recurvature (Fig. 5c) and positive and negative average Rossby wave relative speed over the 72 h following recurvature (Fig. 6c), which are both calculated from the control forecasts of the large-scale flow and have been cited by previous studies to potentially impact the downstream flow (Harr and Elsberry 2000; Agusti-Panareda et al. 2004; Riemer and Jones 2010; Grams et al. 2013a; Keller et al. 2014; Quinting and Jones 2016; Brannan and Chagnon 2020). This section will compare the normalized ensemble standard deviation of PV through differences in the composites between the upper tercile (or positive subgroup) and the lower tercile (or negative subgroup). The null hypothesis is that there is no difference in the predictability (i.e., the ensemble standard deviation) of the PV distribution between the upper and lower (or positive and negative) subsets for each characteristic plotted in Figs. 4, 5c, and 6c. The null hypothesis is rejected for a given characteristic at a specific time and location if the difference between the composite standard deviations of the subsets is not contained by the 95% confidence interval created from 2000 bootstrap replicates. Note that each subplot of Figs. 4, 5c, and 6c displays the subgroup differences in the normalized ensemble standard deviation for the forecast cycle that is initialized 24 h before recurvature. These trends, though, are persistent through many initialization times especially before recurvature, therefore this forecast cycle can be considered representative of any forecast cycle initialized prior to recurvature.

The subsets created strictly based on TC characteristics at the time of recurvature (Figs. 4a–e) exhibit comparatively smaller areas of significant predictability differences between

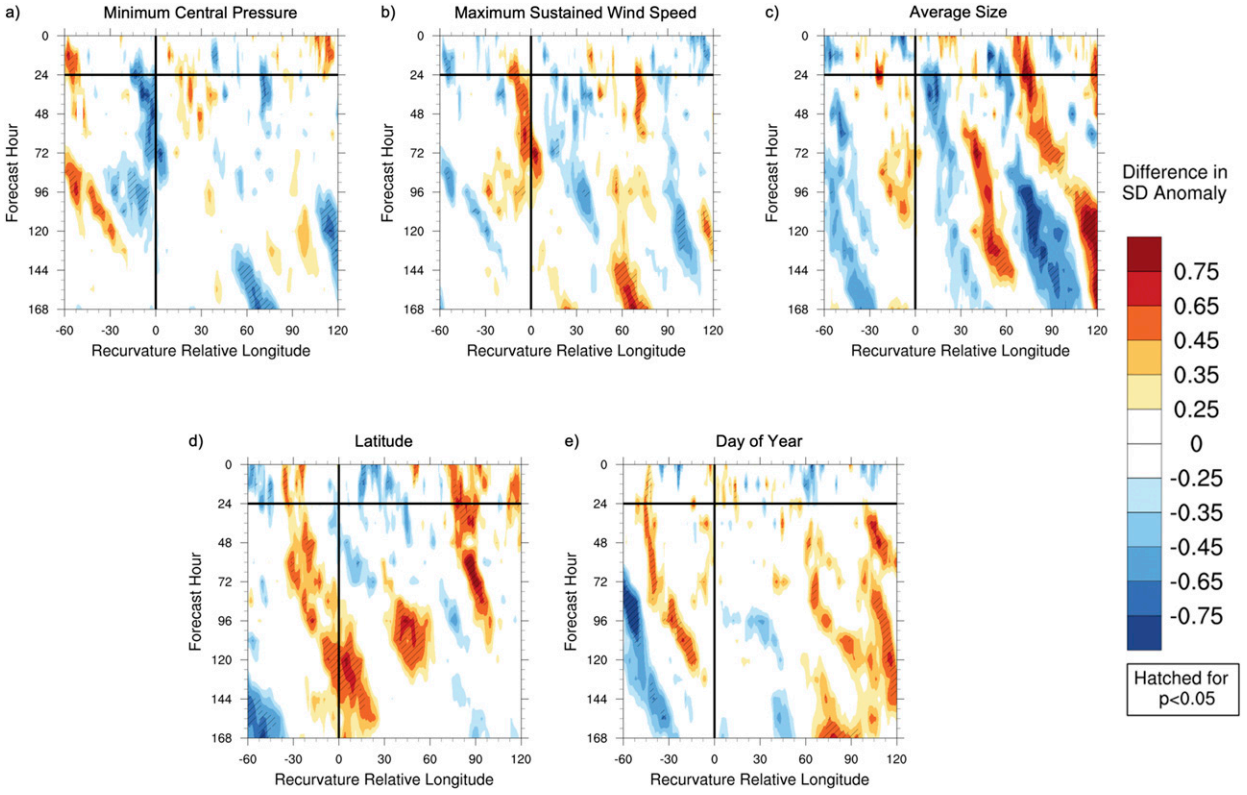

FIG. 4. Color shading illustrates the difference in the normalized standard deviation anomalies of PV on the 320-K isentropic surface for the forecast cycle initialized 24 h before recurvature, calculated by subtracting the lower-tercile composite from the upper-tercile composite, which are determined from the TC's (a) minimum central pressure, (b) maximum sustained wind speed, (c) average size, (d) latitude, and (e) date at the point of recurvature. The thick vertical and horizontal lines denote the recurvature longitude and time, respectively. Hatching indicates times/locations where anomalies are statistically significant from climatology at the 95% confidence level.

the high and low terciles. This is consistent with their lack of influence on the downstream flow response shown in Brannan and Chagnon (2020). The upper tercile of the TC's recurvature pressure encompassed 28 TCs with a minimum central pressure greater than 1005 hPa, and the lower tercile consisted of 24 storms with pressures less than 991 hPa. As can be inferred from the inverse relationship between a TC's minimum central pressure and its maximum sustained wind speed, similar subsets were created for maximum sustained wind speed at the time of recurvature—26 cases in the upper tercile with wind

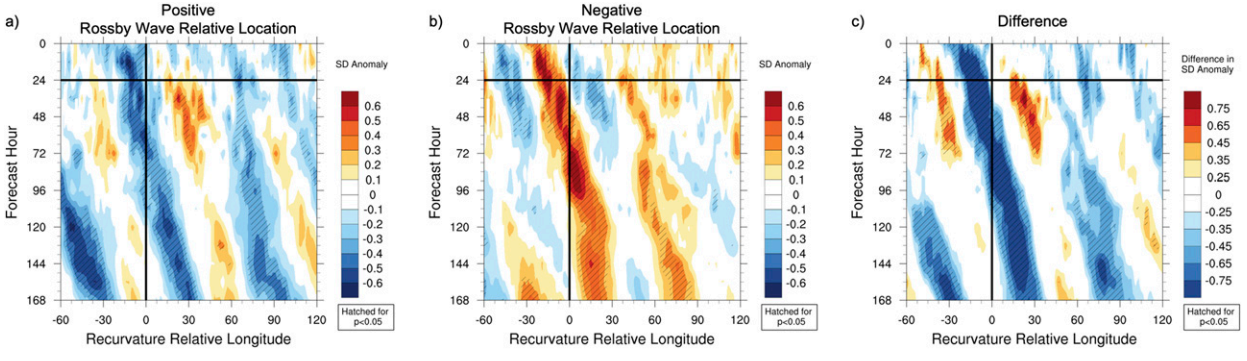

FIG. 5. The normalized standard deviation anomalies of PV (color shading) on the 320-K isentropic surface for the forecast cycle initialized 24 h before recurvature for the (a) positive and (b) negative subgroups created from the value of each case's Rossby wave relative location. (c) The difference (color shading) between subgroups, calculated by subtracting the negative composite in (b) from the positive composite in (a). The thick vertical and horizontal lines denote the recurvature longitude and time, respectively. Hatching indicates times/locations where anomalies are statistically significant from climatology at the 95% confidence level.

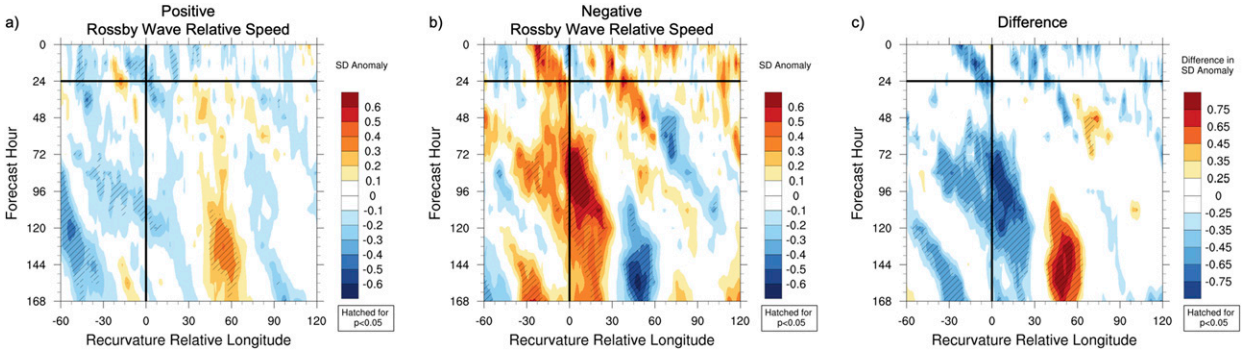

FIG. 6. As in Fig. 5, but for the subsets created from positive and negative Rossby wave relative speed.

speeds greater than 55 kt and 28 cases in the lower tercile with wind speeds less than 35 kt. Figure 4a shows the differences in the predictability for the upper and lower subsets created according to minimum central pressure, which are essentially the opposite signs but same trends as those present for the maximum wind speed subsets in Fig. 4b. The only notable, though still small, differences in the predictability of the PV field for the two subsets of these characteristics occur in the first 48 h following recurvature between 15° upstream and 5° downstream of the recurvature longitude. Within this area, the stronger TCs (lower central pressure or higher maximum wind subsets) are associated with an ensemble standard deviation that is statistically greater than climatology with 95% confidence.

The influence of the size of TC at recurvature is investigated in Fig. 4c where the upper tercile is created from the 18 largest TCs with an average 34-kt wind radii greater than 127.6 n mi (1 n mi = 1.852 km) and is compared with the lower-tercile composite from the 18 smallest TCs with an average 34-kt wind radii below 65 n mi. While there are some areas of significant differences between the standard deviations of these two subsets downstream from recurvature, they are small in area and longevity. The areas of alternating positive and negative significant differences between 45° and 120° downstream over the 96–144 forecast hours (72–120 h after recurvature) are related to standard deviation anomalies that zonally alternate above and below the climatological average and are longitudinally offset between the upper and lower terciles. This pattern may be linked to differences between the terciles in their average phasing with the large-scale ridges and troughs.

The latitude (Fig. 4d) and day (Fig. 4e) of recurvature are selected as subgrouping characteristics based on the seasonal dependence of the extratropical jet's position and strength. Seasonal shifts of the jet in combination with the range of recurvature latitudes create setups with closer and farther TC–jet interactions, motivating this study to investigate any potential influence of the jet's seasonality on the downstream predictability. The upper latitude composite is created from those TCs that recurve northward of 30.8°N and the lower latitude composite averages over cases with recurvatures southward of 26.6°N. The main differences between the predictability of these subsets occur over three separate 36-h periods that begin at forecast hour 108 (84 h after recurvature) and near the recurvature longitude, forecast hour 84 (60 h after recurvature) and 45° downstream, and forecast hour 54 (30 h after recurvature) and 90° downstream. In each of these locations, the cases with a more northward recurvature latitude have a significantly larger ensemble standard deviation of PV relative to the more southern recurvature cases. In fact, in each of these areas, the ensemble standard deviation of the northward subset is significantly greater than the climatological average, indicating worse-than-average predictability, at the 95% confidence level. Conversely, there very few areas of significant predictability differences between the northern and southern recurvature subsets aligned with the time of recurvature. The subsets based on the recurvature day of year select those storms recurving after 15 September as the upper-tercile cases and those recurving before 18 August as the lower-tercile cases. There are small areas of significant differences between the subgroups that allude to the later recurvature cases having significantly greater standard deviations relative to the early recurvature cases. These areas, however, coincide with areas in which the early recurvature subgroup has better-than-average predictability (a negative standard deviation anomaly) with 95% confidence. This could be linked to the summertime extratropical jet, which tends to be weaker and more zonal. There are not any areas, however, that are positioned along the recurvature longitude or verification time.

c. *Composites over subsets based on TC/Rossby wave phasing*

The Rossby wave relative location and speed are calculated based on the positioning between the TC and "trough of interest," which is the nearest trough to the TC at the time of recurvature. The Rossby wave relative location (used as the subgrouping metric for Fig. 5c) is calculated for each case at the time of recurvature by subtracting the TC's recurvature longitude from the longitude of the trough of interest. It is essentially the zonal distance between the trough of interest and the TC at the point of recurvature, which is illustrated by Fig. 8 of Brannan and Chagnon (2020). Here, the cases are grouped based on positive and negative Rossby wave relative locations that correspond to TCs recurving on the west or east side of the nearest trough, respectively. Figure 5c shows several large areas of significant differences in uncertainty between these subsets. The standard deviation difference with the longest duration begins 30° upstream and 24 h before recurvature and

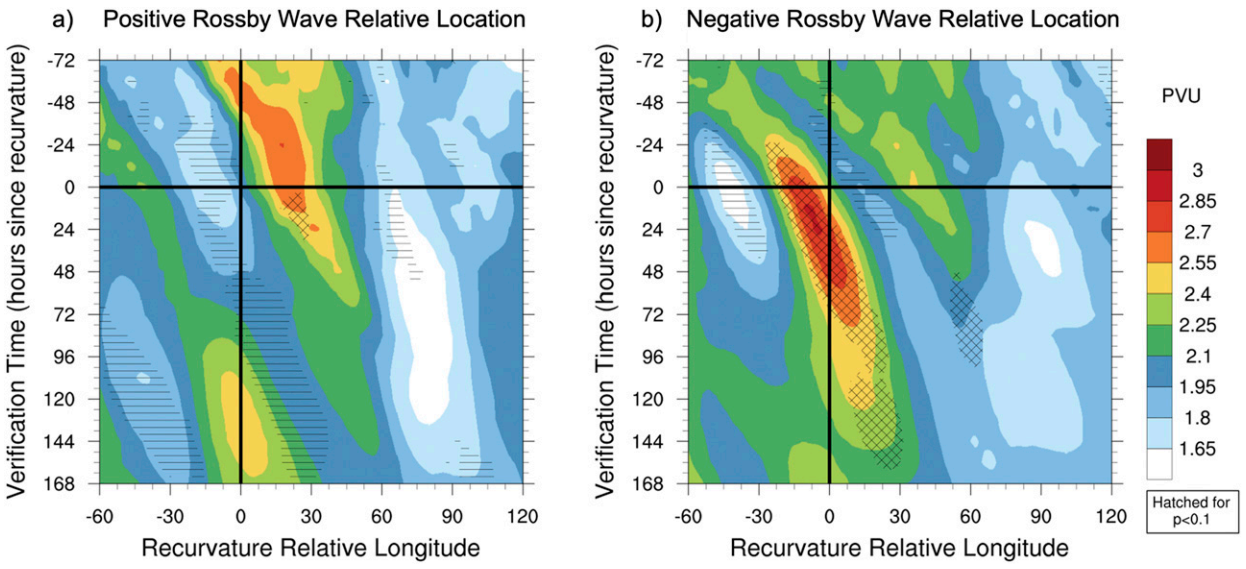

FIG. 7. Potential vorticity on 320-K isentropic surface (color shading) and significant standard deviation anomalies (hatching) calculated from an average of all forecast cycles spanning from 168 h before recurvature to the time of recurvature, aligned according to verification time, for subsets of TCs with a (a) positive and (b) negative Rossby wave relative location at the time of recurvature. Horizontal hatching and full cross hatching respectively highlight the areas where the normalized standard deviation anomalies of PV on the 320-K isentropic surface are statistically less than or greater than climatology at the 90% confidence level. The thick vertical and horizontal lines denote the recurvature longitude and time, respectively.

propagates with time, reaching 30° downstream 144 h after recurvature (corresponding to a forecast hour of 168 at the plotted initialization time). As shown in Fig. 5b (Fig. 5a), this area of significance is tied to an area of significantly above (below) average standard deviation in the negative (positive) Rossby wave relative location subset, which would also correspond to the location of an upstream trough (ridge) by the definition of this characteristic. Similarly, the other large areas with significantly negative differences occur from −50° to −20° upstream and about 60°–90° downstream, which, again, are collocated with areas of above (below) average standard deviation in the negative (positive) Rossby wave relative location subset. Alternatively, the areas of significantly positive differences in Fig. 5c that begin near the time of recurvature from −45° to −30° upstream and from 15° to 30° downstream can be attributed to the areas with significantly larger (smaller) ensemble standard deviations relative to climatology in the positive (negative) Rossby wave relative location subset, apparent by the colored contours representing the standard deviation anomalies in Figs. 5a and 5b. These alternating areas of significantly above- and below-average standard deviations in each subset individually appear to be anchored to the time of recurvature as well as the phase of the propagating Rossby wave, which will become more clear in the discussion of Fig. 7.

The final subsetting characteristic is the Rossby wave relative speed, plotted in Fig. 6. This metric is computed by subtracting the zonal displacement of the TC in the 72 h following recurvature from the zonal displacement of the trough of interest during the same time period. A positive Rossby wave relative speed describes the cases in which the trough moves farther eastward, (i.e., zonally faster) relative to the TC, and a negative Rossby wave relative speed groups the cases with TCs that traverse greater eastward distances than their nearest troughs. The differences in ensemble standard deviation between these subgroups are mainly contained by three areas. The largest difference by area is approximately centered along the recurvature longitude and extends from forecast hour 48 (24 h after recurvature) through forecast hour 168 (144 h after recurvature). Appearing as a significantly negative anomaly in Fig. 6c, the positive Rossby wave relative speed cases experience significantly better predictability (less ensemble standard deviation) in this area relative to the cases with negative Rossby wave relative speeds. While some of this area corresponds to an ensemble standard deviation significantly less than climatology in the positive Rossby wave relative speed cases (Fig. 6a), nearly this entire area is characterized by an ensemble standard deviation significantly greater than climatology in the negative Rossby wave relative speed cases (Fig. 6b). The position of elevated uncertainty within the negative Rossby wave relative speed cases could be physically explained by a trough whose zonal propagation lags behind the TC, potentially yielding greater variance among ensemble members close to the recurvature longitude in the days following recurvature. It is important to note that this subset does not necessarily imply that the troughs of interest in these negative Rossby wave cases are slower than average; it may also characterize cases where the TC propagates faster than average, or some combination of both. The tercile comparison of standard deviation differences was also executed separately for the zonal speed of the TC and of the trough in the 72 h after recurvature; however, the resulting composites were incredibly similar to their respective categories of Rossby wave relative

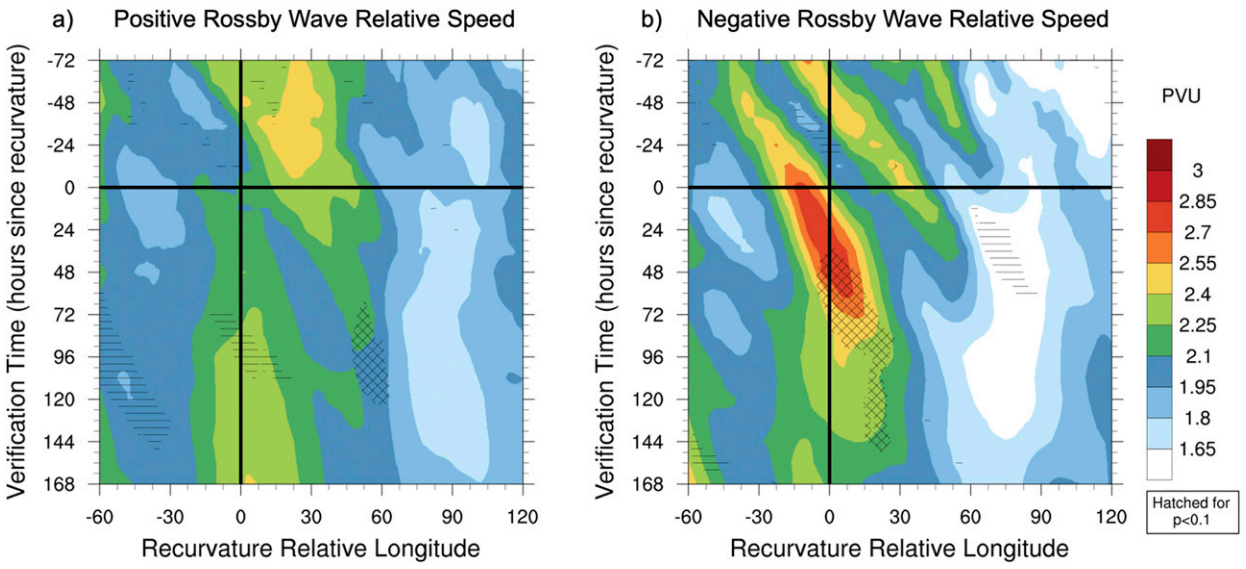

FIG. 8. As in Fig. 7, but for the subsets created from positive and negative Rossby wave relative speed.

speeds, and are therefore omitted here. As depicted by Fig. 6c, there is also an area of significantly positive difference between the predictability of the positive and negative Rossby wave relative speed subsets that is situated between 40° and 60° downstream beginning at forecast hour 96 (72 h after recurvature), signifying an area where the positive Rossby wave relative speed cases have significantly more uncertainty in their PV forecasts than those cases with negative Rossby wave relative speed. The roots of this difference are traced to the same area in Figs. 6a and 6b where the negative Rossby wave relative speed cases exhibit predictability significantly better than climatology whereas the positive Rossby wave relative speed cases show significantly decreased predictability relative to climatology. Again, these trends may be related to the trough location/propagation and the intrinsic uncertainty associated with them. In the positive Rossby wave relative speed subset, the trough of interest travels faster downstream than the TC, which could be contributing to the above-average standard deviation anomaly nearly 60° downstream.

The differences between the subsets of the phasing characteristics shown in Figs. 6c and 5c are not only significant, but they are also larger in area and longer-lived trends than seen from the subset differences based solely on TC characteristics (Figs. 4a–e). Therefore, the predictability differences based on these two characteristics will be the focus of the remainder of this study.

The pattern and evolution of standard deviation exhibits a strong relationship to the recurvature time and location, as demonstrated in Figs. 7 and 8. In fact, this relationship exists regardless of the specific forecast lead time when recurvature takes place. To highlight this relationship, the remaining figures are composited in the following way. Instead of compositing according to the forecast hour, we composite according to the recurvature relative verification time. In this approach, a range of forecast lead times contribute to each recurvature relative verification time in the composite. Unlike Figs. 4–6, which only present the forecast valid at the $T - 24$ initialization time, the remaining figures display signals that are robust over forecasts from initialization times $T - 168$ to $T + 0$. The combination of each initialization time and each forecast hour allows the forecasts from every forecast cycle to be shifted and aligned according to their verification time. Once aligned by their verification times, averages are taken over each forecast cycle to result in a distribution of ensemble standard deviation (including areas of significant differences from climatology) and ensemble averaged PV as a function of recurvature relative verification time and longitude. This technique reliably synthesizes the forecasts from the individual initialization times to produce a field displaying standard deviation and PV signals that are common to the range of forecast cycles and highlight the trends linked to TC recurvature. Note that the confidence interval was slightly lowered for these plots relative to that in Figs. 4, 5c, and 6c to account for the expectation that averaging over various forecast cycles could reduce the magnitude of some standard deviation anomalies.

Given the relationship between the areas of significantly anomalous standard deviations and the hypothesized trough/ridge locations based on the defining characteristics of Rossby wave relative location and speed, Figs. 7 and 8 display the areas of significantly enhanced or diminished ensemble standard deviations alongside the ensemble averaged PV. The connection between predictability and the trough and ridge locations for the Rossby wave relative location subsets is demonstrated in Fig. 7. The positive Rossby wave relative speed subset (Fig. 7a) is characterized by an upstream ridge at the time of recurvature, shown by the area of low PV that lies in the largest area of lower-than-average standard deviation, both of which propagate together downstream. The other ridges present in this subset (from −60° to −30° upstream and from 60° to 90° downstream) also show signs of predictability that is statistically better than climatology. The one area of significantly greater ensemble standard deviation is small and occurs

in the 36 h after recurvature, approximately 30° downstream. This downstream area of heightened uncertainty appears to be linked to the changing magnitude of the downstream trough. Similar trends are exemplified by the negative Rossby wave relative speed subset (Fig. 7b). The trough of interest in the negative Rossby wave relative speed subset is located upstream from the recurvature longitude as illustrated by the area of elevated PV. This upstream trough is also collocated with the largest area of the significantly greater-than-average ensemble standard deviation, indicating the greatest uncertainty is tied to the upstream trough, which subsequently propagates downstream, carrying the decreased predictability with it. Both areas of significantly better predictability at the time of recurvature (from −45° to −30° upstream and from 0° to 30° downstream) are aligned along ridge axes. The final area of significance is not as clearly tied to a trough or ridge axis. It indicates significantly greater-than-average standard deviation 48–96 h after recurvature, approximately 60° downstream. This area may be tied to uncertainty in a weakening downstream trough as it is situated at a location corresponding to a diminishing positive PV anomaly.

This subset was specifically created based on the phase of the Rossby waves at the time of recurvature, which would naturally better align the position of troughs and ridges between cases and could contribute to the enhanced significance displayed for this subset. A question that remains is to what extent is the predictability associated with uncertainty in the location of troughs and ridges versus the amplitude? To investigate this question, we investigate the TC's affect on the predictability of Rossby wave amplitude, which is reported in section 4.

The same averaging technique employed in producing Fig. 7 is executed for the Rossby wave relative speed subsets shown in Fig. 8. As expected, due to more trough/ridge position variance within these subsets, there are fewer areas of predictability that are significantly different from climatology. Nevertheless, the predictability trends are, in fact, quite different between the subsets. With that being said, the distributions of average PV between these subsets is roughly similar—a trough axis along the recurvature longitude, another trough between 0° and 60° downstream, and a ridge between 60° and 120° downstream. The magnitudes of the troughs and ridges in combination with the standard deviation anomalies for the positive Rossby wave relative speed composite (Fig. 8a) are smaller than those for the negative subset (Fig. 8b). A potential explanation for this difference is the larger sample size for the positive Rossby wave relative speed subgroup (N = 48) than for the negative subgroup (N = 24). Consistent with Fig. 6, averaging over the range of initialization times does not dismiss the area of significantly reduced standard deviation centered along the recurvature longitude, 72–108 h after recurvature. In this case though, the better-than-average predictability is also collocated with a trough position, which is a different association than seen so far. The area of increased uncertainty located 60° downstream, roughly 72–120 h after recurvature, is not perfectly aligned with a trough axis, as previously hypothesized, which may also be the result of a reduction in the magnitude of PV maxima from averaging over a large subset of storms. This reduction of predictability, though, may be still be related to uncertainty in the position of the trough of interest or its changing magnitude.

In the negative Rossby wave relative speed composite (Fig. 8b), there is an area of significantly elevated standard deviation beginning near the recurvature longitude 36 h after recurvature, which propagates downstream through 144 h after recurvature. This anomaly is aligned with the trough axis that begins upstream at the time of recurvature; however, it appears to be related to uncertainty in the simulated amplitude changes as the trough begins to diminish. The area of reduced standard deviation 60°–90° downstream between 12 and 60 h following recurvature lies well within the large downstream ridge. The entire ridge, though, is not characterized by significantly better predictability, therefore this area too may be related to discrepancies between ensemble members in simulating amplitude changes to the downstream ridge following recurvature.

To differentiate between the predictability related to Rossby wave position versus amplitude, the following section will investigate the large-scale uncertainty following TC recurvature events within spectral space to emphasize amplitude uncertainties.

4. Spectral space results

This section explores the large-scale uncertainty associated with Atlantic recurvature events by analyzing the standard deviation of the total power derived from wavelet decompositions of the Rossby wave metric from each ensemble member. The total power isolates the amplitude of the Rossby wave train and is not sensitive to the precise location of ridge and trough axes. By evaluating the uncertainty in forecasts of total power, we are thus able to evaluate whether TC recurvature affects the predictability of the Rossby wave amplitude. The normalization method described in section 2d and employed throughout section 3 to normalize the standard deviations across all seasons, forecast hours, and locations is utilized again here, but using climatological values based on wavelet standard deviation averages. The wavelet power as well as the locations and times where the standard deviation is significantly different from climatology is plotted in Figs. 9 and 10 according to the Rossby wave relative location and speed subgroups, respectively. To emphasize the persistent signals across forecast cycles initialized between $T - 168$ and $T + 0$, the same averaging technique used in Figs. 7 and 8 is used in Figs. 9 and 10 to illustrate trends as a function of recurvature relative verification time and longitude.

a. *Rossby wave relative location*

There are stark differences in the predictability of Rossby wave amplitude following recurvature events with positive (Fig. 9a) and negative (Fig. 9b) Rossby wave relative locations. Though the positive Rossby wave relative location subset's downstream response appears to be weaker than that of the negative subset, the two separate composites have somewhat similar trends in downstream power, which is not surprising given that this characteristic was insignificant in differentiating between downstream responses in Brannan and Chagnon (2020). Despite the similarity in power, there are significant

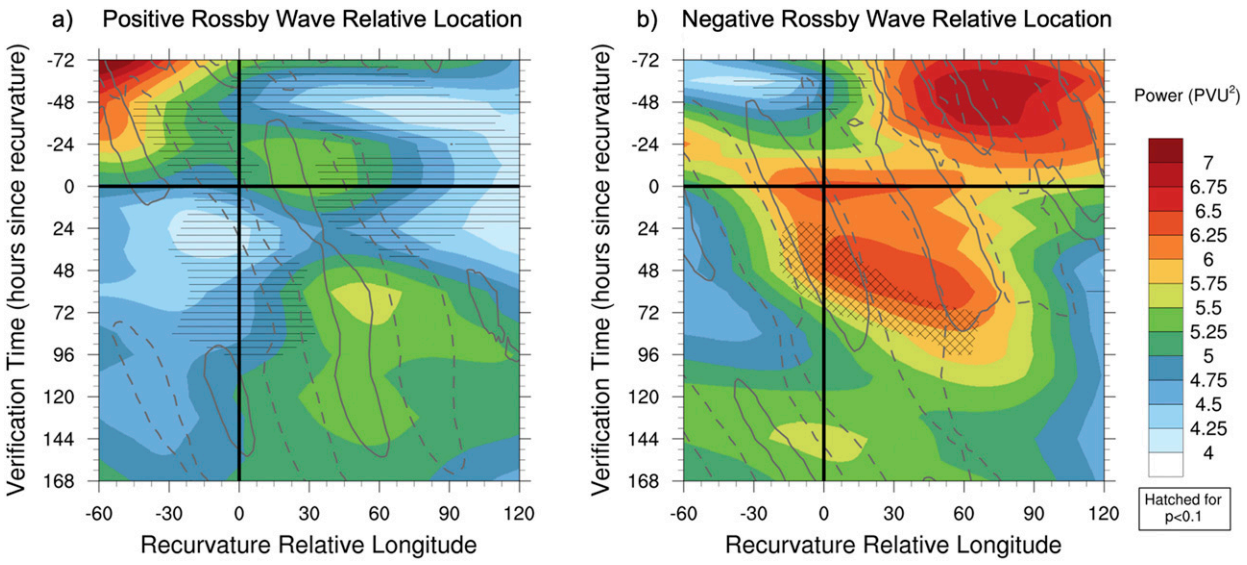

FIG. 9. Total power (color shading), significant standard deviation anomalies (hatching), trough power maxima (solid gray contours), and ridge power maxima (dashed gray contours) calculated from an average of all forecast cycles spanning from 168 h before recurvature to the time of recurvature, aligned according to verification time, for subsets of TCs with a (a) positive or (b) negative Rossby wave relative location at the time of recurvature. Horizontal hatching and full cross hatching respectively highlight the areas where the normalized standard deviation anomalies of total power are statistically less than or greater than climatology at the 90% confidence level. The gray lines contour the areas of trough (solid) and ridge (dashed) power above 2.5 PVU^2. The thick vertical and horizontal lines denote the recurvature longitude and time, respectively.

differences in the predictability trends between these subsets. The positive Rossby wave relative location subset (Fig. 9a), in fact, shows several areas of below-average wavelet standard deviations, corresponding to increased predictability. These areas of significantly better-than-average predictability are aligned with changes to the local minima in total power, situated from −30° to 30° and centered in time at 24 h after recurvature as well as from 0° to 120° downstream from $T - 72$ to $T + 36$. The large-scale response to recurvature is weaker overall for this subset relative to that of the negative Rossby wave relative location subset. This difference is expected since a positive Rossby wave relative location case implies that a TC is positioned to the west of the nearest upper-level trough, which is typically correlated with a weaker interaction between the TC and the extratropical flow. Results from Fig. 9a indicate that these Rossby wave amplitudes are also

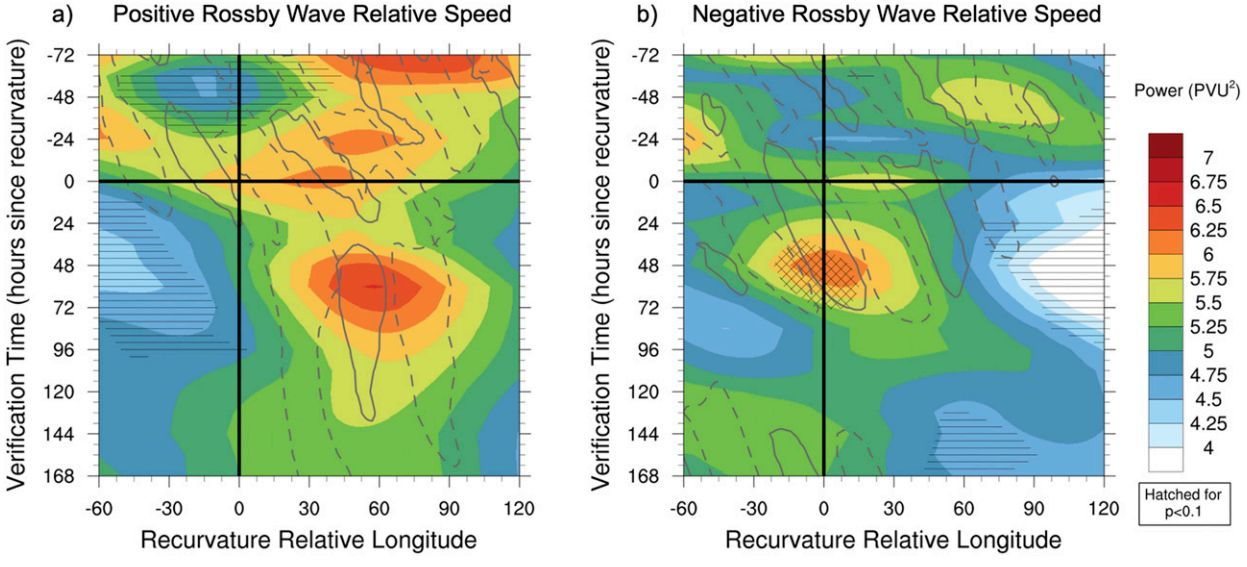

FIG. 10. As in Fig. 9, but for the subsets created from positive and negative Rossby wave relative speed.

statistically equivalent to or better than the climatological average of ensemble standard deviation.

The negative Rossby wave relative location subset (Fig. 9b) is characterized by a plume of significantly increased wavelet standard deviation that emerges near 15° upstream and 24 h after recurvature and propagates rather quickly downstream, reaching 60° downstream by 72 h after recurvature. Though this uncertainty arises at a longitude and time aligned with the trough axis connected to the upstream trough at the time of recurvature, the plume of decreased predictability propagates downstream faster than the trough. The uncertainty in the wavelet power is more clearly tied to magnitude changes of the total wavelet power—specifically, the decrease in power that occurs over the 60° downstream of recurvature in the 48–96 h after recurvature. The increases in power near the time of recurvature over the same downstream region do not yield predictability trends that are significantly different from climatology (and neither do the increases or decreases in power associated with the downstream power maxima centered in time at about 48 h before recurvature). The downstream increase in power that is initiated near the time and longitude of recurvature along with its associated area of decreased predictability is likely tied to this subset's synoptic setup in which a TC positioned just eastward of an upper-level trough at the time of recurvature facilitates a strong TC–trough interaction by baroclinic processes. The amplitudes of the Rossby waves resulting from these baroclinic growth processes appear to be less predictable than the climatological average based on their ensemble standard deviations, which is a result consistent with those from an analysis of the western North Pacific by Quinting and Jones (2016).

b. *Rossby wave relative speed*

Consistent with the results of Brannan and Chagnon (2020), which used a larger set of TCs from a different reanalysis dataset, the downstream Rossby wave response following recurvature is much different between the positive and negative Rossby wave relative speed subsets as shown by the colored contours of total wavelet power composites in Fig. 10. The positive Rossby wave relative speed cases (Fig. 10a) are characterized by an increase in 0°–120° downstream Rossby wave power (for both troughs and ridges) that peaks at 60 h after recurvature. This increase in power, though, is not associated with trends in predictability that are significantly different than climatology. Therefore, the process regulating amplification is relatively predictable and not likely related to an instability. The negative Rossby wave relative speed cases (Fig. 10b) exhibit an increase in wavelet power centered on the recurvature longitude and peaking about 48 h after recurvature, while there is a simultaneous decrease in wavelet power 60°–120° downstream that arises near the recurvature time. The increase in power along the recurvature longitude is collocated with an area of significantly greater ensemble standard deviation relative to climatology (reduced predictability) and is also aligned with a trough axis that is just upstream of the TC at recurvature. Therefore, the increased ensemble spread in total power at synoptic-scale wavelengths is linked to Rossby wave amplification following recurvature, which may be attributed to baroclinic processes. Conversely, the downstream power minima following recurvature is associated with a significantly less-than-average ensemble standard deviation and is most likely governed by barotropic processes, which is further discussed in section 5.

5. Summary and discussion

Recurving tropical cyclones are known to interact with the extratropical jet and affect the synoptic-scale flow downstream (Harr and Dea 2009; Grams et al. 2011; Archambault et al. 2013, 2015; Grams and Archambault 2016; Pohorsky et al. 2019; Brannan and Chagnon 2020). Given this ability of TCs to disturb the synoptic-scale extratropical flow, a natural question to ask is whether the predictability is also modified? The focus of the analysis presented in this paper was to determine if and how the predictability of the synoptic-scale extratropical flow is disturbed by recurving TCs in the Atlantic basin. A similar analysis has been conducted by Torn (2017) in which it was demonstrated that the uncertainty in ensemble-based forecasts is indeed enhanced when transition occurs upstream of a large amplitude ridge. Torn (2017) also showed that the forecast uncertainty was unaffected by the presence of an upstream trough or by uncertainty in the initial position of the TC, among other factors. This paper is distinguished from and elaborates on Torn (2017) in several ways. First, whereas Torn (2017) analyzed the predictability of 500-hPa heights, this paper analyzes a Rossby wave metric based on isentropic PV. The justification for analyzing isentropic PV is that it is a natural field for tracking the dynamics of Rossby waves. While a TC does introduce perturbations to isentropic PV, the evolution of isentropic PV near the extratropical jet is dominated by Rossby waves. As such, the analysis in this paper is focused on the predictability of Rossby waves that dominate the propagation of downstream effects. Second, following Brannan and Chagnon (2020), this paper evaluates the influence of the relative propagation speed of Rossby waves and TCs in regulating the predictability. This paper also evaluates the predictability in both physical space and in spectral space. Using wavelet transforms, the analysis of the spectral predictability permits the distinction between predictability of the phase (i.e., locations of troughs and ridges) and the predictability of Rossby wave amplitude. The primary findings from this analysis are summarized as follows:

- Predictability is degraded when recurvature occurs downstream of a trough (e.g., see Figs. 7b and 9b). The associated increase in ensemble spread is largest in the upstream trough itself, which subsequently communicates the degraded predictability downstream. Conversely, predictability is enhanced (i.e., the ensemble spread is reduced) when recurvature takes place downstream of a ridge (e.g., see Figs. 7a and 9a). This result opposes that from Torn (2017) who found no significant difference in the downstream ensemble spread between Atlantic recurvature cases with and without an upstream trough.
- Predictability is degraded when the Rossby wave train propagates more slowly than the recurving TC (e.g., see

Fig. 8b). The resulting increase in ensemble spread is largest and persists near the longitude of recurvature.

- The modification of ensemble spread is anchored in time and space to the recurvature of the TC. In other words, the pattern of modification depends much less on the forecast lead time than it does on the instance of recurvature.
- TC recurvature is associated with a statistically significant increase in the uncertainty of Rossby wave amplitude. This increase is most pronounced when recurvature occurs downstream of a trough (Fig. 9b) or when the TC propagates faster than the Rossby wave pattern (Fig. 10b).
- The uncertainty in Rossby wave amplitude is distinct from that associated with the phase, the latter of which is affected by the location of ridges and troughs. This difference is most evident when comparing Figs. 7b and 9b. The uncertainty in amplitude (Fig. 9b) spans the entire wave train from east to west, encompassing the upstream trough, the downstream ridge, and a downstream trough.

The characteristics of the predictability differ from those of the dynamical Rossby wave response as presented in Brannan and Chagnon (2020). Most notably, Brannan and Chagnon (2020) showed that the resulting extratropical flow response is most strongly linked to the relative speeds of the TC and the Rossby wave train in the 72 h after recurvature. Though this study utilizes an alternative PV dataset and contains fewer TCs, the respective trends between the Rossby wave relative speed and the downstream, postrecurvature wave amplitude remain consistent with Brannan and Chagnon (2020). The most common TC–Rossby wave configuration involves a Rossby wave that travels faster downstream than the TC (i.e., a positive Rossby wave relative speed), which is shown by Brannan and Chagnon (2020) and Fig. 10a to yield a statistically significant increase in the synoptic-scale Rossby wave amplitude downstream from and after the time of recurvature. Conversely, when a TC moves faster than the Rossby wave train (i.e., for negative Rossby wave relative speeds; Fig. 10b), there is an initial suppression of downstream wave amplitude (apparent at longitudes greater than 60°) for several days following recurvature before the amplitude returns to climatological values. Though positive/negative Rossby wave relative speeds yield distinct differences in their downstream trends in Rossby wave amplitude, this study reveals that neither downstream response is subject to increased ensemble spread and uncertainty (e.g., see Fig. 10). Furthermore, Brannan and Chagnon (2020) demonstrated only a weak connection between Rossby wave amplification and the location of the nearest trough at the recurvature time. In stark contrast, this paper has shown that the uncertainty is most enhanced when a trough exists upstream at the time of recurvature (e.g., see Fig. 9b). This apparent contradiction is discussed in the following paragraph.

We hypothesize that the ensemble spread and uncertainty are largest when and where baroclinic processes are most active. On the other hand, Rossby wave amplitude changes that are driven by barotropic processes are not accompanied by a significant loss of predictability. With regard to TC–Rossby wave interactions, baroclinic processes are most active during the time of extratropical transition. The extratropical transition occurs most vigorously when the upper-level Rossby wave pattern is optimally phased with the TC (i.e., when a trough is located upstream). This is precisely the time, location, and configuration that results in the largest forecast uncertainty as demonstrated in this paper. This uncertainty may then be communicated downstream and may affect Rossby wave amplitude across a wave pattern spanning the basin (e.g., see Fig. 9b). In contrast, barotropic interaction effects are not associated with increased uncertainty. For example, Brannan and Chagnon (2020) hypothesized that the large changes in wave amplitude downstream of a fast moving TC (i.e., negative Rossby wave relative speed) were due to the barotropic interaction between the Rossby wave and the TC vortex (i.e., the TC vortex acts as a surrogate for an edge wave, and the tilt of the combined TC–Rossby wave pattern with the shear would imply destructive interference). This barotropic process is more predictable (see Fig. 10b) than the baroclinic processes characteristic of extratropical transition, despite similar changes in Rossby wave amplitude between the two referenced areas. The two referenced areas include 1) the colored contours in Fig. 10b that show increasing power with time (orange contours near recurvature) overlaid with above-average standard deviations and 2) decreasing power with time (white contours 90° downstream from recurvature) overlaid with below-average standard deviations. The magnitude of the changes in power for these two areas are similar. While consistent with the evidence presented in this paper, a complete test of this hypothesis is beyond the scope of the present climatological study.

The composite analysis of forecast predictability presented in this paper required the specification of 1) the time at which interaction between the TC and Rossby waves begins, and 2) a field that best serves as a proxy for identifying the Rossby wave response. Neither of these two concepts can be embodied by a single, precise, one-size-fits-all metric that is appropriate for all events included in our analysis. We have used the recurvature time and PV on the 320-K isentropic surface. As noted in section 2a, whether normalizing by the time of recurvature, extratropical transition, or maximum interaction as determined by the upper-level PV advection by the irrotational wind, it is expected that these times fall within 36 h of each other. Although we cannot confidently detect significant changes on time scales shorter than this time period, this study focuses on trends that persist on time scales approaching 1 week for which significance was demonstrated. Nevertheless, it is likely that these modifications to predictability have their origin in processes whose time scale is indeed shorter (e.g., baroclinic growth during transition and the related growth of error). Future investigations that focus on these shorter-time-scale processes should carefully consider what is the most appropriate means of standardizing the time at which interaction begins. Concerning the use of PV on the 320-K isentropic surface, we acknowledge that this level is typically found at elevations well below the tropopause at latitudes that are equatorward of the extratropical jet. However, our analysis focuses on Rossby waves on the extratropical jet. The 320-K surface reliably intersects the tropopause at a latitude near the

extratropical jet. Nevertheless, several questions remain unanswered. How deeply do the signals diagnosed in this paper extend above the 320-K surface? How much of the signal we observe at the 320-K isentropic level is contributed by Rossby wave breaking events, cutoff lows, and PV streamers? These questions have begun to be investigated in the context of case studies (i.e., Baumgart and Riemer 2019) but should be further interrogated from a climatological standpoint in future work.

Although not addressed directly in this study, diabatic processes may play a significant role in regulating the interaction between TCs and the extratropical jet. PV is modified by diabatic processes such as latent heating and radiative cooling in TCs. The diabatically modified PV may be transported by the irrotational wind away from the TC and toward the extratropical jet. Grams et al. (2011) demonstrated that such processes played a key role in modifying the upper-level Rossby waveguide in an event that led to downstream Rossby wave breaking. Diabatic processes may also play an important role in intensifying the irrotational outflow from TCs. Hitchman and Rowe (2019) argued that mesoscale outflow jets in TCs are of diabatic origin, forming as a result of the horizontal PV dipole mechanism described by Chagnon and Gray (2009). Given that diabatic tendencies are associated with small-scale and/or parameterized processes that are subject to large uncertainty, future work should address the potential role of diabatic processes in governing the predictability of the TC–Rossby wave interaction.

Future studies should also investigate whether the variability in the position of the trough of interest, magnitude of the trough of interest, or the forecast Rossby wave relative speed impacts the downstream trends in ensemble standard deviation. The analysis in this study focused on the effects of recurving Atlantic TCs on the ensemble forecasts of downstream Rossby waves; however, an equally important aspect of predictability that should be evaluated in a future study concerns the error (i.e., the bias) of the ensemble mean in its forecasts of downstream Rossby waves. An investigation into forecast error would also benefit from analyses in both physical and spectral space in order to differentiate between phase and amplitude errors.

Estimating the uncertainty inherent to a forecast is of immense value to forecasters and stakeholders alike. Great strides have been made in the design of operational ensemble weather predictions systems that can deliver this information. Nevertheless, the physical and dynamical factors that govern the uncertainty of a particular forecast remains an active area of research. Forecasts of TCs are themselves subject to a large degree of uncertainty due to the complexity, instability, and nonlinear nature of their genesis and evolution. Rossby waves, on the other hand, are subject to less uncertainty due to their synoptic-scale nature. When TCs interact with a preexisting Rossby wave train, how does the uncertainty of the TC affect that of the Rossby wave pattern? This study has provided evidence that the Rossby wave pattern is affected to varying degrees depending on the precise nature of the interaction, with baroclinically dominated interactions being the most likely means of enhancing the uncertainty.

Acknowledgments. The authors thank the reviewers for insightful feedback that significantly enhanced this paper. We acknowledge the National Hurricane Center for compiling and providing their Best Track reanalysis database. We also thank the European Centre for Medium-Range Weather Forecasts for contributing global archived forecast data on isentropic surfaces.

REFERENCES

Agusti-Panareda, A., C. D. Thorncroft, G. C. Craig, and S. L. Gray, 2004: The extratropical transition of Hurricane Irene (1999): A potential-vorticity perspective. *Quart. J. Roy. Meteor. Soc.*, **130**, 1047–1074, https://doi.org/10.1256/qj.02.140.

Aiyyer, A., 2015: Recurving western North Pacific tropical cyclones and midlatitude predictability. *Geophys. Res. Lett.*, **42**, 7799–7807, https://doi.org/10.1002/2015GL065082.

Anwender, D., P. A. Harr, and S. C. Jones, 2008: Predictability associated with the downstream impacts of the extratropical transition of tropical cyclones: Case studies. *Mon. Wea. Rev.*, **136**, 3226–3247, https://doi.org/10.1175/2008MWR2249.1.

——, S. C. Jones, M. Leutbecherb, and P. A. Harr, 2010: Sensitivity experiments for ensemble forecasts of the extratropical transition of Typhoon Tokage (2004). *Quart. J. Roy. Meteor. Soc.*, **136**, 183–200, https://doi.org/10.1002/qj.527.

Archambault, H. M., L. F. Bosart, D. Keyser, and J. M. Cordeira, 2013: A climatological analysis of the extratropical flow response to recurving western North Pacific tropical cyclones. *Mon. Wea. Rev.*, **141**, 2325–2346, https://doi.org/10.1175/MWR-D-12-00257.1.

——, D. Keyser, L. F. Bosart, C. A. Davis, and J. M. Cordeira, 2015: A composite perspective of the extratropical flow response to recurving western North Pacific tropical cyclones. *Mon. Wea. Rev.*, **143**, 1122–1141, https://doi.org/10.1175/MWR-D-14-00270.1.

Baumgart, M., and M. Riemer, 2019: Processes governing the amplification of ensemble spread in a medium-range forecast with large forecast uncertainty. *Quart. J. Roy. Meteor. Soc.*, **145**, 3252–3270, https://doi.org/10.1002/qj.3617.

Brannan, A. L., and J. M. Chagnon, 2020: A climatology of the extratropical flow response to recurving Atlantic tropical cyclones. *Mon. Wea. Rev.*, **148**, 541–558, https://doi.org/10.1175/MWR-D-19-0216.1.

Chaboureau, J.-P., F. Pantillon, D. Lambert, E. Richard, and C. Claud, 2012: Tropical transition of a Mediterranean storm by jet crossing. *Quart. J. Roy. Meteor. Soc.*, **138**, 596–611, https://doi.org/10.1002/qj.960.

Chagnon, J. M., and S. L. Gray, 2009: Horizontal potential vorticity dipoles on the convective storm scale. *Quart. J. Roy. Meteor. Soc.*, **135**, 1392–1408, https://doi.org/10.1002/qj.468.

Cordeira, J. M., and L. F. Bosart, 2010: The antecedent large-scale conditions of the "perfect storms" of late October and early November 1991. *Mon. Wea. Rev.*, **138**, 2546–2569, https://doi.org/10.1175/2010MWR3280.1.

Evans, J. L., J. M. Arnott, and F. Chiaromonte, 2006: Evaluation of operational model cyclone structure forecasts during extratropical transition. *Mon. Wea. Rev.*, **134**, 3054–3072, https://doi.org/10.1175/MWR3236.1.

Grams, C. M., and H. M. Archambault, 2016: The key role of diabatic outflow in amplifying the midlatitude flow: A representative case study of weather systems surrounding western North Pacific extratropical transition. *Mon. Wea. Rev.*, **144**, 3847–3869, https://doi.org/10.1175/MWR-D-15-0419.1.

——, and Coauthors, 2011: The key role of diabatic processes in modifying the upper-tropospheric wave guide: A North Atlantic case-study. *Quart. J. Roy. Meteor. Soc.*, **137**, 2174–2193, https://doi.org/10.1002/qj.891.

——, S. C. Jones, C. A. Davis, P. A. Harr, and M. Weissmann, 2013a: The impact of Typhoon Jangmi (2008) on the midlatitude flow. Part I: Upper-level ridgebuilding and modification of the jet. *Quart. J. Roy. Meteor. Soc.*, **139**, 2148–2164, https://doi.org/10.1002/qj.2091.

——, ——, and ——, 2013b: The impact of Typhoon Jangmi (2008) on the midlatitude flow. Part II: Downstream evolution. *Quart. J. Roy. Meteor. Soc.*, **139**, 2165–2180, https://doi.org/10.1002/qj.2119.

Harr, P. A., and R. L. Elsberry, 2000: Extratropical transition of tropical cyclones over the western North Pacific. Part I: Evolution of structural characteristics during the transition process. *Mon. Wea. Rev.*, **128**, 2613–2633, https://doi.org/10.1175/1520-0493(2000)128<2613:ETOTCO>2.0.CO;2.

——, and J. M. Dea, 2009: Downstream development associated with the extratropical transition of tropical cyclones over the western North Pacific. *Mon. Wea. Rev.*, **137**, 1295–1319, https://doi.org/10.1175/2008MWR2558.1.

——, D. Anwender, and S. C. Jones, 2008: Predictability associated with the downstream impacts of the extratropical transition of tropical cyclones: Methodology and a case study of Typhoon Nabi (2005). *Mon. Wea. Rev.*, **136**, 3205–3225, https://doi.org/10.1175/2008MWR2248.1.

Hitchman, M. H., and S. M. Rowe, 2019: On the structure and formation of UTLS PV dipole/jetlets in tropical cyclones by convective momentum surges. *Mon. Wea. Rev.*, **147**, 4107–4125, https://doi.org/10.1175/MWR-D-18-0232.1.

Hoskins, B. J., M. E. McIntyre, and A. W. Robertson, 1985: On the use and significance of isentropic potential vorticity maps. *Quart. J. Roy. Meteor. Soc.*, **111**, 877–946, https://doi.org/10.1002/qj.49711147002.

Jones, S. C., and Coauthors, 2003: The extratropical transition of tropical cyclones: Forecast challenges, current understanding, and future directions. *Wea. Forecasting*, **18**, 1052–1092, https://doi.org/10.1175/1520-0434(2003)018<1052:TETOTC>2.0.CO;2.

Keller, J. H., S. C. Jones, and P. A. Harr, 2014: An eddy kinetic energy view of physical and dynamical processes in distinct forecast scenarios for the extratropical transition of two tropical cyclones. *Mon. Wea. Rev.*, **142**, 2751–2771, https://doi.org/10.1175/MWR-D-13-00219.1.

Klein, P. M., P. A. Harr, and R. L. Elsberry, 2002: Extratropical transition of western North Pacific tropical cyclones: Midlatitude and tropical cyclone contributions to reintensification. *Mon. Wea. Rev.*, **130**, 2240–2259, https://doi.org/10.1175/1520-0493(2002)130<2240:ETOWNP>2.0.CO;2.

Landsea, C. W., and J. L. Franklin, 2013: Atlantic hurricane database uncertainty and presentation of a new database format. *Mon. Wea. Rev.*, **141**, 3576–3592, https://doi.org/10.1175/MWR-D-12-00254.1.

Lorenz, E. N., 1965: A study of the predictability of a 28-variable atmospheric model. *Tellus*, **17**, 321–333, https://doi.org/10.3402/tellusa.v17i3.9076.

——, 1995: Predictability: A problem partly solved. *Seminar on Predictability*, ECMWF, Shinfield Park, Reading, United Kingdom, 18 pp., https://www.ecmwf.int/node/10829.

Martius, O., C. Schwierz, and H. C. Davies, 2010: Tropopause-level waveguides. *J. Atmos. Sci.*, **67**, 866–879, https://doi.org/10.1175/2009JAS2995.1.

Nielsen-Gammon, J. W., 2001: A visualization of the global dynamic tropopause. *Bull. Amer. Meteor. Soc.*, **82**, 1151–1167, https://doi.org/10.1175/1520-0477(2001)082<1151:AVOTGD>2.3.CO;2.

Pantillon, F., J.-P. Chaboureau, C. Lac, and P. Mascart, 2013: On the role of a Rossby wave train during the extratropical transition of Hurricane Helene (2006). *Quart. J. Roy. Meteor. Soc.*, **139**, 370–386, https://doi.org/10.1002/qj.1974.

Pohorsky, R., M. Röthlisberger, C. M. Grams, J. Riboldi, and O. Martius, 2019: The climatological impact of recurving North Atlantic tropical cyclones on downstream extreme precipitation events. *Mon. Wea. Rev.*, **147**, 1513–1532, https://doi.org/10.1175/MWR-D-18-0195.1.

Quinting, J. F., and S. C. Jones, 2016: On the impact of tropical cyclones on Rossby wave packets: A climatological perspective. *Mon. Wea. Rev.*, **144**, 2021–2048, https://doi.org/10.1175/MWR-D-14-00298.1.

Reynolds, C. A., M. S. Peng, and J.-H. Chen, 2009: Recurving tropical cyclones: Singular vector sensitivity and downstream impacts. *Mon. Wea. Rev.*, **137**, 1320–1337, https://doi.org/10.1175/2008MWR2652.1.

Riemer, M., and S. C. Jones, 2010: The downstream impact of tropical cyclones on a developing baroclinic wave in idealized scenarios of extratropical transition. *Quart. J. Roy. Meteor. Soc.*, **136**, 617–637, https://doi.org/10.1002/qj.605.

——, ——, and C. A. Davis, 2008: The impact of extratropical transition on the downstream flow: An idealized modelling study with a straight jet. *Quart. J. Roy. Meteor. Soc.*, **134**, 69–91, https://doi.org/10.1002/qj.189.

Swinbank, R., and Coauthors, 2016: The TIGGE project and its achievements. *Bull. Amer. Meteor. Soc.*, **97**, 49–67, https://doi.org/10.1175/BAMS-D-13-00191.1.

Torn, R. D., 2017: A comparison of the downstream predictability associated with ET and baroclinic cyclones. *Mon. Wea. Rev.*, **145**, 4651–4672, https://doi.org/10.1175/MWR-D-17-0083.1.

——, and G. J. Hakim, 2015: Comparison of wave packets associated with extratropical transition and winter cyclones. *Mon. Wea. Rev.*, **143**, 1782–1803, https://doi.org/10.1175/MWR-D-14-00006.1.

Torrence, C., and G. P. Compo, 1998: A practical guide to wavelet analysis. *Bull. Amer. Meteor. Soc.*, **79**, 61–78, https://doi.org/10.1175/1520-0477(1998)079<0061:APGTWA>2.0.CO;2.